SUPPLEMENTAL DATA

XRCC4 INTERACTIONS WITH XRCC4-LIKE FACTOR (XLF) CREATE AN EXTENDED GROOVED SCAFFOLD FOR DNA LIGATION AND DOUBLE-STRAND BREAK REPAIR

Michal Hammel[1], Martial Rey[2], Yaping Yu[2], Rajam S. Mani[3], Scott Classen[1], Mona Liu[1], Michael E. Pique[4], Shujuan Fang[2], Brandi Mahaney[2], Michael Weinfeld[3], David C. Schriemer[2], Susan P. Lees-Miller[2] and John A. Tainer[4,5]

[1]Physical Biosciences Division, Lawrence Berkeley National Laboratory, Berkeley, CA 94720, USA, [2]Department of Biochemistry and Molecular Biology and the Southern Alberta Cancer Research Institute, University of Calgary, Calgary, Alberta T2N 4N1, Canada, [3]Department of Oncology, University of Alberta and the Cross Cancer Institute, Edmonton, Alberta T6G 1Z2, Canada, [4]Department of Molecular Biology, Skaggs Institute of Chemical Biology, The Scripps Research Institute, La Jolla, CA 92037, USA, [5]Life Sciences Division, Lawrence Berkeley National Laboratory, Berkeley, CA 94720, USA

Table of contents:

Table S1. Data collection and refinement statistics for the crystal structure of the XLF^{1-224}-$XRCC4^{1-140}$ complex.

Data collection

Space group	$P6_522$
Cell Dimensions (Å)	
a=b, c	110.0, 763.7
Wavelength (Å)	1.0
Resolution range (Å)	70-3.97
Observations	635,287
Unique reflections	25218
<I/σ>	
Total	16.75
shell (4.71-4.58)	6.15
shell (4.58-4.47)	4.31
shell (4.47-4.37)	4.38
shell (4.37-4.28)	3.07
shell (4.28-4.19)	2.71
shell (4.19-4.11) [a]	1.93
shell (4.11-4.04)	1.64
Final shell (4.04-3.97) [b]	1.25
R_{SYM} (%)	
Total	15.2
shell (4.71- 4.58)	91.8
Completeness (%)	
Total	99.7
Final shell (4.06-3.97)	99.3

Refinement

a)	Resolution range (Å)	67-4.11	
	Number of reflections	20122	
	R_{work}/ R_{free} [b]		35.0 / 36.3
b)	Resolution range (Å)	67-3.97	
	Number of reflections	21776	
	R_{work}/ R_{free} [b]		35.7 / 36.9

Number of refined atoms 11369

The R_{work}/ R_{free} was calculated for two resolution limits a) 4.11 and b) 3.97Å.

Figure S1

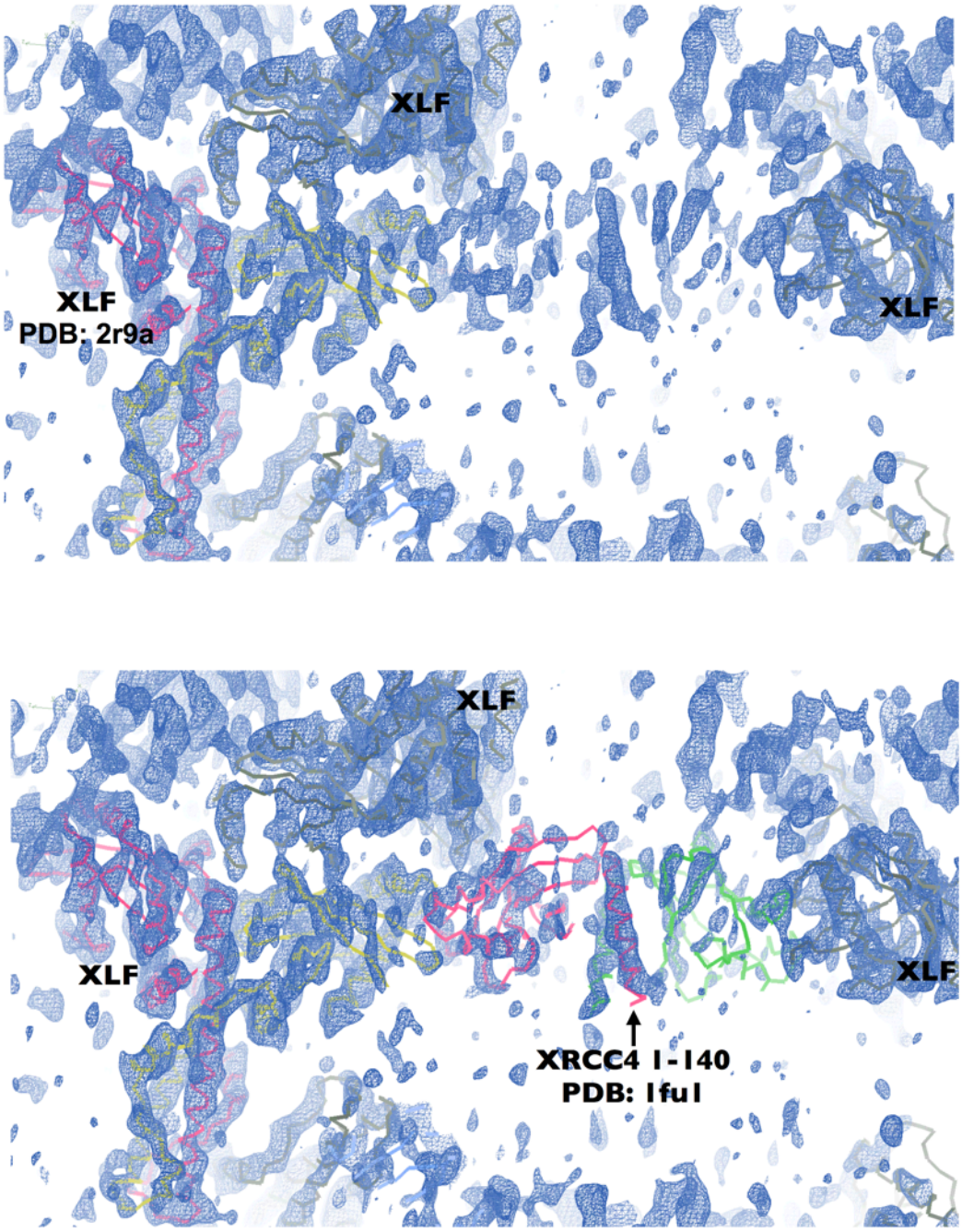

Figure S1. Initial phasing. Electron density map at 4.50Å resolution limit after XLF$^{1-224}$ was placed by molecular replacement allowed visualization of the electron density for XRCC4$^{1-140}$. The electron density of the 2Fo-Fc map for the initial phase is shown contoured at 1.5σ. Crystallographic statistics are shown in Table S1.

Figure S2

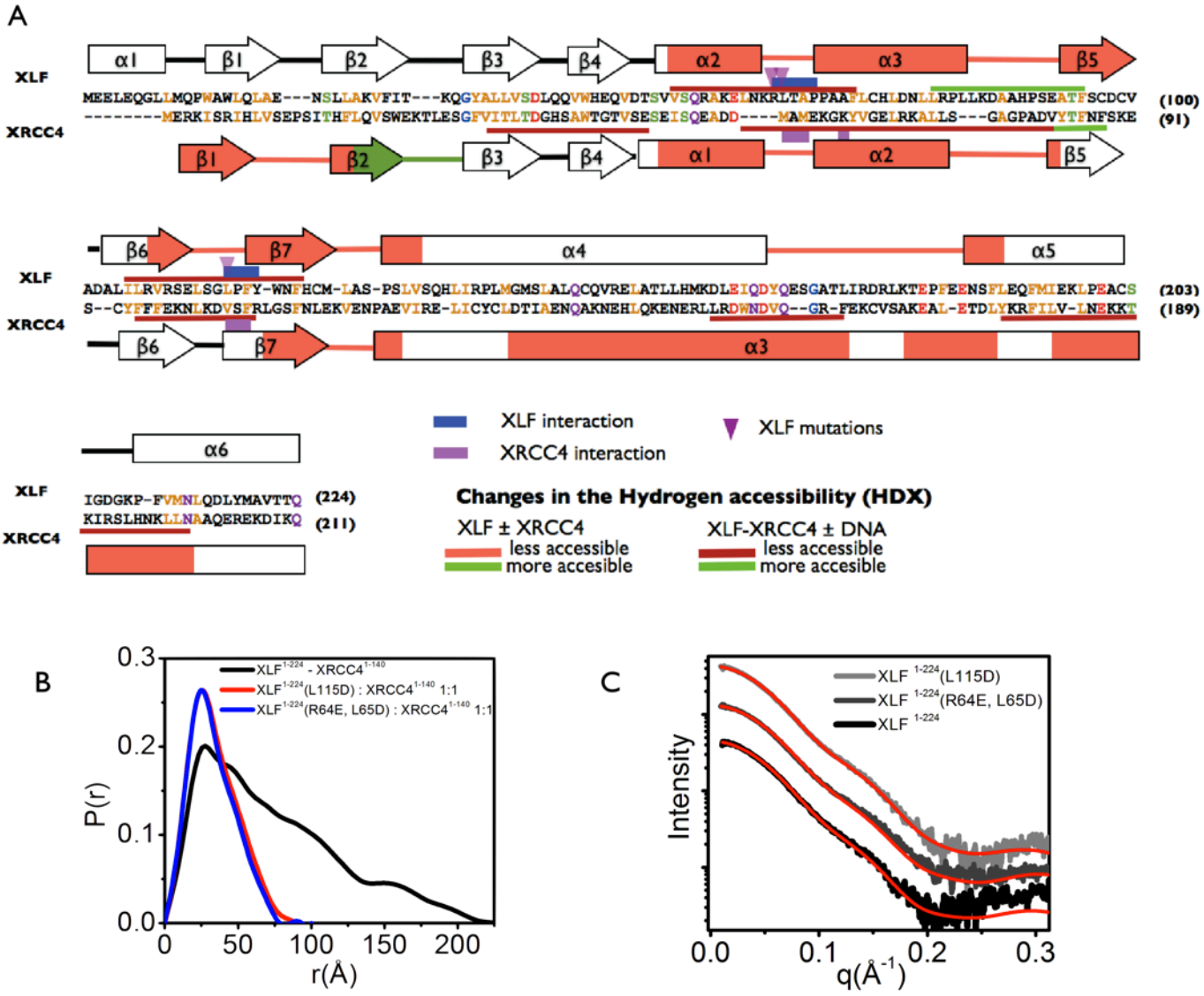

Figure S2. Molecular interaction of XLF with XRCC4. (A) Structure-based sequence alignment of XLF$^{1–224}$ and XRCC4$^{1–211}$. Conserved residues defined in (1,2) are colored by: hydrophobic, yellow; negative charge, red; positive charge, blue; proline and glycine, brown; threonine and serine, green; cysteine, light blue; and glutamine and asparagine, purple. XLF-XRCC4 interactions based on the crystal structure presented in Figure 1 are highlighted with blue and purple lines. Amino acids that undergo conformational changes upon complexation and DNA binding are highlighted by coloring the secondary structure elements or underlining the amino acids sequences with red and green, respectively.

(B) XRCC4-binding properties of two site-directed mutants of XLF, $XLF^{1-224(L115D)}$ and $XLF^{1-224\ (R64E,\ L65D)}$. Comparison of the P(r) functions calculated for XLF^{1-224}-$XRCC4^{1-140}$ (black), $XLF^{1-224\ (L115D)}$-$XRCC4^{1-140}$(red) and $XLF^{1-224\ (R64,\ L65D)}$-$XRCC4^{1-140}$(blue) show no interaction of mutant protein with XRCC4.

(C) Experimental SAXS curves for XLF^{1-224} (black), $XLF^{1-224\ (R64,\ L65D)}$ and $XLF^{1-224\ (L115D)}$ with the theoretical scattering profile (red) calculated for the crystal structure of XLF^{1-224} (PDBid : 2r9a). The exact match between experimental and theoretical profiles indicates identical overall structure of the mutants with wild type XLF^{1-224} protein.

Figure S3

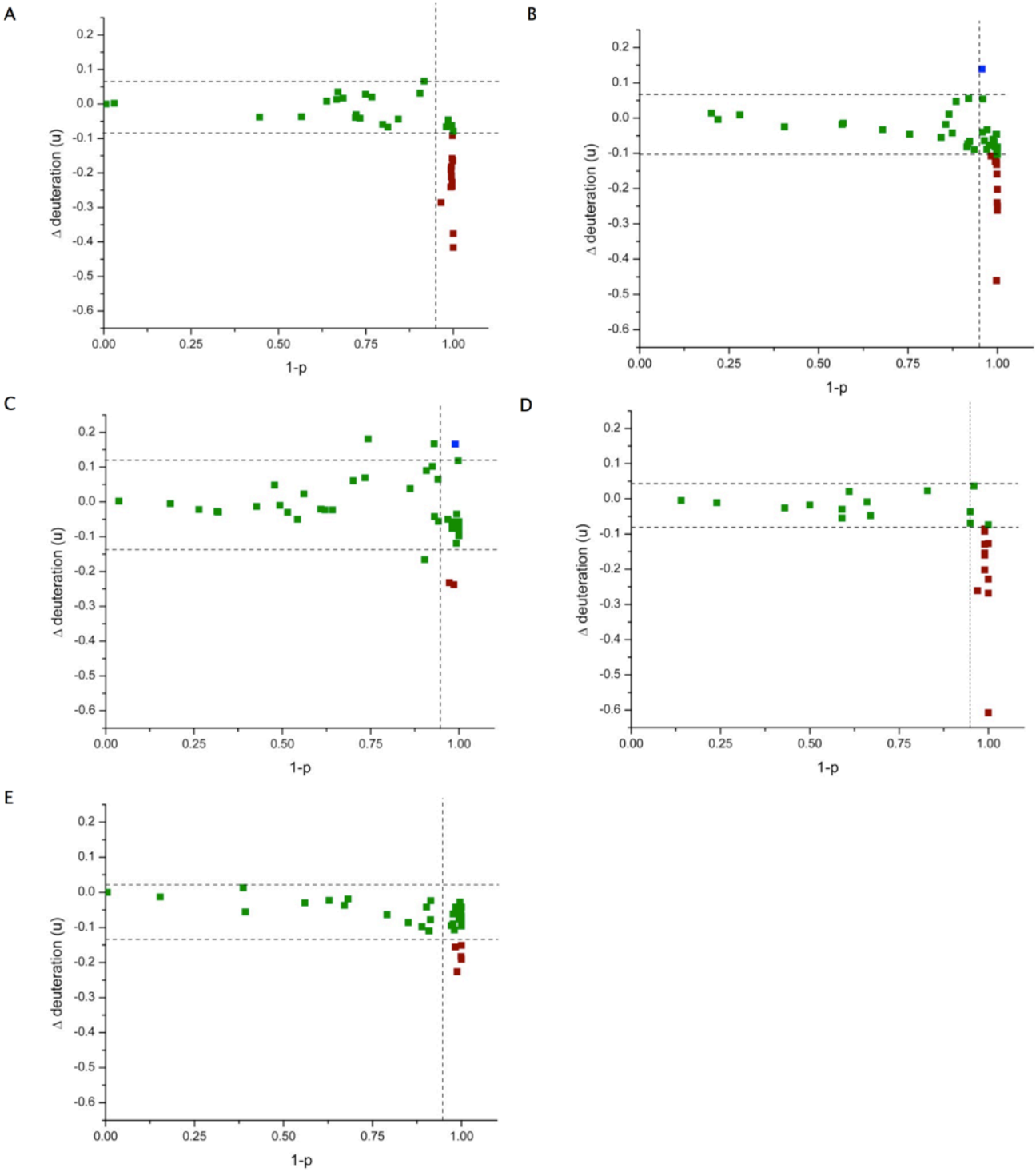
A
B
C
D
E
Δ deuteration (u)
1-p
0.2
0.1
0.0
-0.1
-0.2
-0.3
-0.4
-0.5
-0.6
0.00
0.25
0.50
0.75
1.00

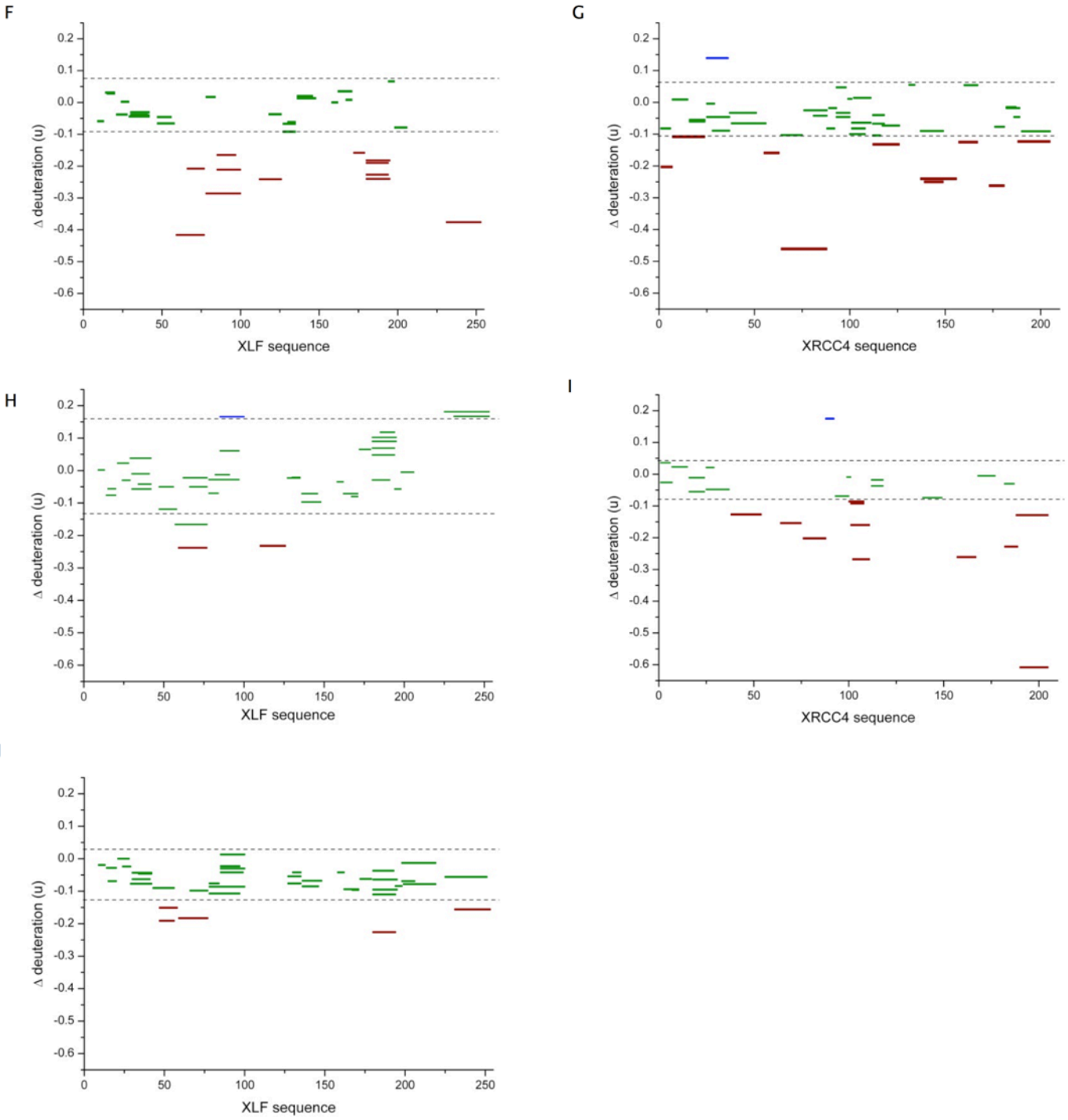

Figure S3. Mass shift measurements.(ABCDE) Mass shift scatterplots arising from combinations of states.(A) mass shifts in XLF upon complexation with XRCC4, (B) mass shifts in XRCC4 upon complexation with XLF, (C) mass shifts in XLF upon complexation of XLF-XRCC4 with 40 bp DNA, (D) mass shifts in XRCC4 upon complexation of XLF-XRCC4 with 40 bp DNA, (E) mass shifts in XLF upon complexation with 40 bp DNA. The horizontal

dotted lines represent ±2 s.d. based on noise in ΔD.(FGHIJ) Sequence plots mapping the mass shifts. (F) mass shifts in XLF upon complexation with XRCC4, (G) mass shifts in XRCC4 upon complexation with XLF, (H) mass shifts in XLF upon complexation of XLF-XRCC4 with 40 bp DNA, (I) mass shifts in XRCC4 upon complexation of XLF-XRCC4 with 40 bp DNA, (J) mass shifts in XLF upon complexation with 40 bp DNA. Significant alterations in peptide mass are represented as red bars, and insignificant shifts in green using criteria described in Supplementary Experimental Procedures. Dashed lines mark the 95% confidence interval for the null hypothesis. The positioning of the bars indicates the location of the pepsin-generated peptides in the protein sequence.

Figure S4

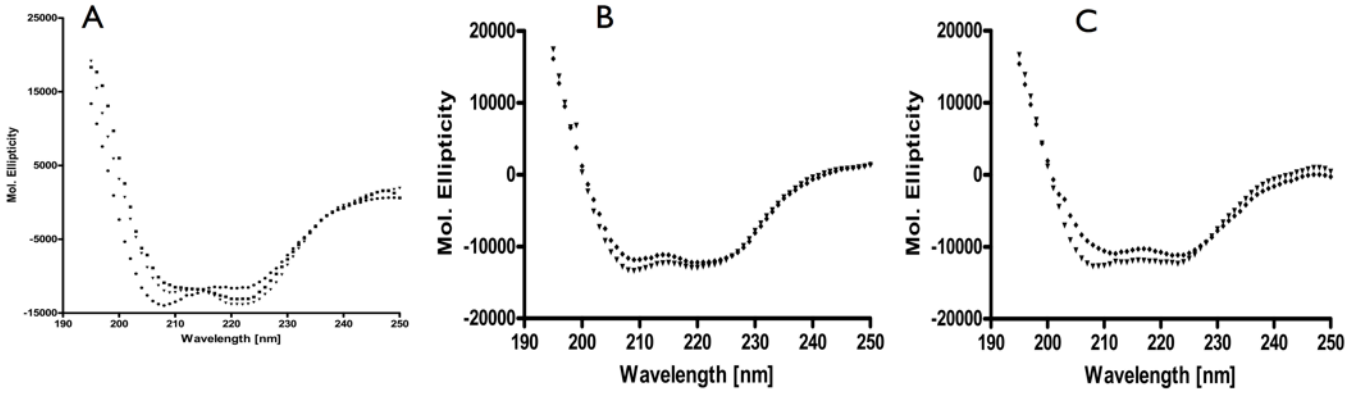

D

Secondary structural analysis of XRCC4, XLF. XLF$^{1-248}$, XRCC4.XLF, and XRCC4.XLF$^{1-248}$ complexes

Protein	Molar ellipticity $[\theta]_{209\ nm}$	Molar ellipticity $[\theta]_{222nm}$	α-Helix	β-structure	Random
XRCC4	-13800	-11500	35	35	30
XLF	-12230	-13840	44	30	26
XLF$^{1-248}$	-11600	-12950	42	25	33
[XRCC4.XLF][a]	-11800	-12100 (E)[b]			
	-13500	-12700 (T)	40	24	36
[XRCC4.XLF$^{1-248}$][a]	-10200	-11200 (E)			
	-12700	-12300 (T)	38	22	40

[a] The two proteins in the XRCC4.XLF and XRCC4.XLF$^{1-248}$ mixtures were mixed in a 1:1 molar ratio.

[b] (E) represents experimental values, and (T) represents theoretical values assuming no protein-protein interaction.

Figure S4. Interaction of XRCC4 with XLF leads to a conformational change in both proteins. (A) Far-UV-CD spectrum of XRCC4 (●, 0.54 mg/ml), XLF (▼, 0.47 mg/ml), and XLF$^{1-248}$ (■, 0.45 mg/ml). (B) Far-UV-CD spectrum of the XRCC4.XLF complex (♦, 0.44 mg/ml) and the theoretical CD spectrum for an equimolar mixture of the two proteins (▼). (C) Far-UV-CD spectrum of the XRCC4.XLF$^{1-248}$ complex (♦, 0.52 mg/ml) and the theoretical CD spectrum for an equimolar mixture of the two proteins (▼). (D) Summary of secondary structural analysis of XRCC4, XLF. XLF$^{1-248}$, XRCC4.XLF and XRCC4.XLF$^{1-248}$ complexes.

Figure S5

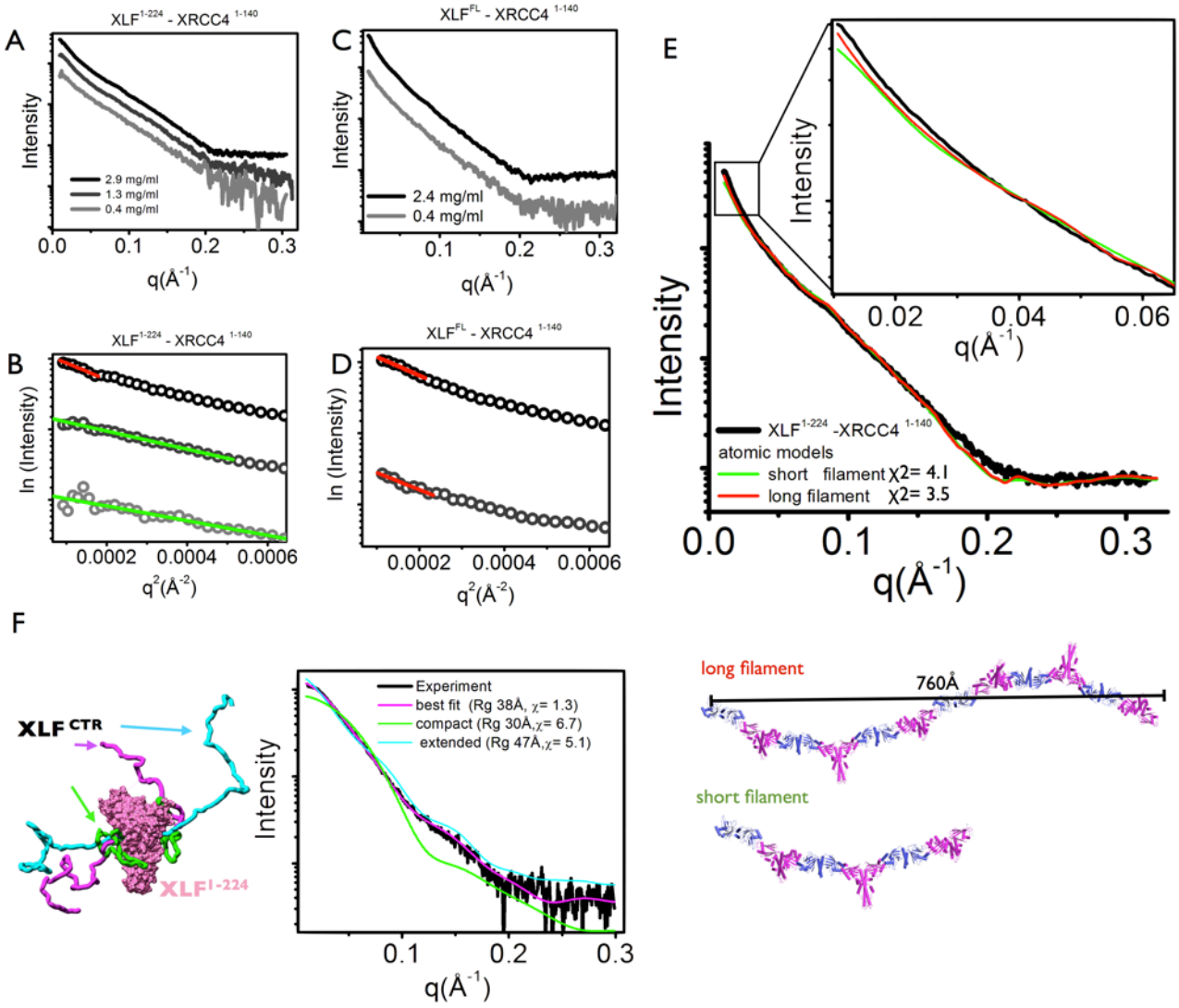

Figure S5. Scattering profiles and Guinier region. (A) SAXS of XLF$^{1-224}$-XRCC4$^{1-140}$ at protein concentrations of 0.4 mg/ml (gray), 1.3 mg/ml (dark gray) and 2.9 mg/ml (black). (B) Guinier plots for SAXS profiles shown in (A) indicating smaller particles for diluted samples. (C) SAXS of XLF^{FL}-XRCC4$^{1-140}$ at protein concentrations of 0.4mg/ml (gray), 2.4mg/ml (black). (D) Guinier plots for SAXS profiles shown in (B) indicating persistence of long XLF^{FL}-XRCC4$^{1-140}$ filaments at low protein concentrations. (E) Formation of long XLF$^{1-224}$-XRCC4$^{1-140}$ filaments at high protein concentration. Experimental scattering profiles for the collected XLF^{FL}-XRCC4$^{1-140}$ fraction at ~2.9 mg/ml. The theoretical scattering (red line, χ^2=3.5) from the short and long filament. The Guinier plot is shown in the panel B. Bottom - Atomic model of XLF^{FL}-XRCC4$^{1-140}$ filaments used in the calculation of the theoretical SAXS. Discrepancy in the fit for the $q<0.05$Å^{-1} indicate the existence of very long filaments with a length longer than larger-

tested filament. (F) Comparison of the theoretical SAXS profiles for the XLF models (shown) with the unfolded C-terminus model (χ^2 = 1.3, magenta line), a globular C-terminus (χ^2 = 6.7, green line) and largely extended C-terminus models (χ^2 = 5.1, cyan line).

Figure S6

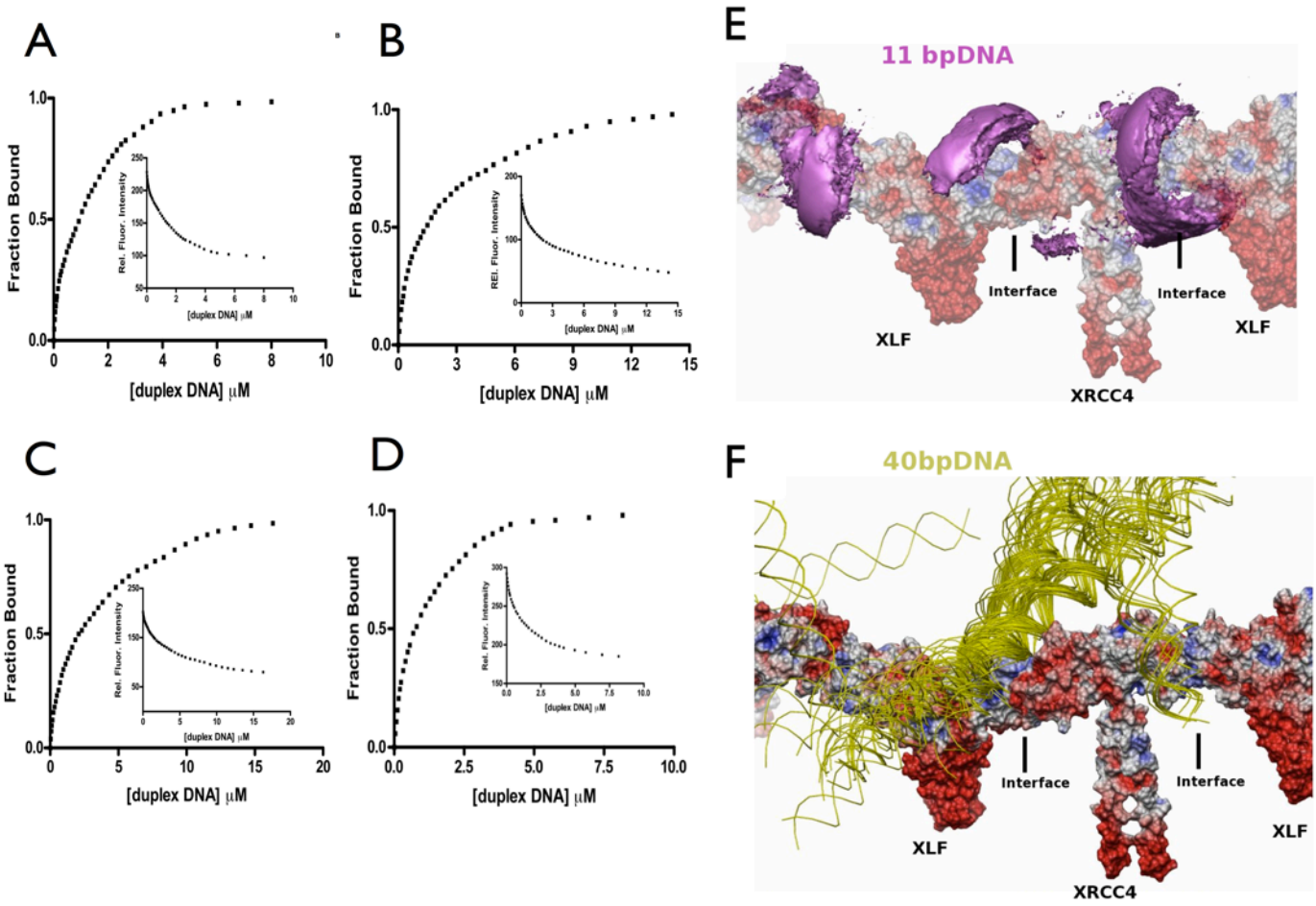

Figure S6. XLF-XRCC4 interaction with DNA. (ABCD) Fluorescence titration of XRCC4, XLF^{FL}, XLF^{1-248} and the XRCC4-XLF^{1-248} complex with duplex [40-mer] DNA. (A) XRCC4 (0.4 μM) (B) XLF (0.5 μM) (C) XLF^{1-248} and (D) the XRCC4-XLF^{1-248} protein complex in 50 mM Tris-HCl, pH 7.5, 100 mM NaCl, 5 mM $MgCl_2$ and 1 mM DTT, were excited at 295 nm, and the fluorescence intensity was monitored at 335 nm (see insets). The fraction bound, i.e. relative fluorescence (Rel. Fluor.) intensity versus ligand concentration, is plotted. (EF) DNA docking. (E) 11bp DNA docking placements are shown as purple blobs. The purple blobs are the favorable locations in the DOT "partition sum" output grid: at each grid point, the 54,000 different DNA orientations are weighted by their energy and summed. (F) 99 top-ranked placements of 40bpDNA (yellow). The protein surface is colored by electrostatic potential.

Figure S7

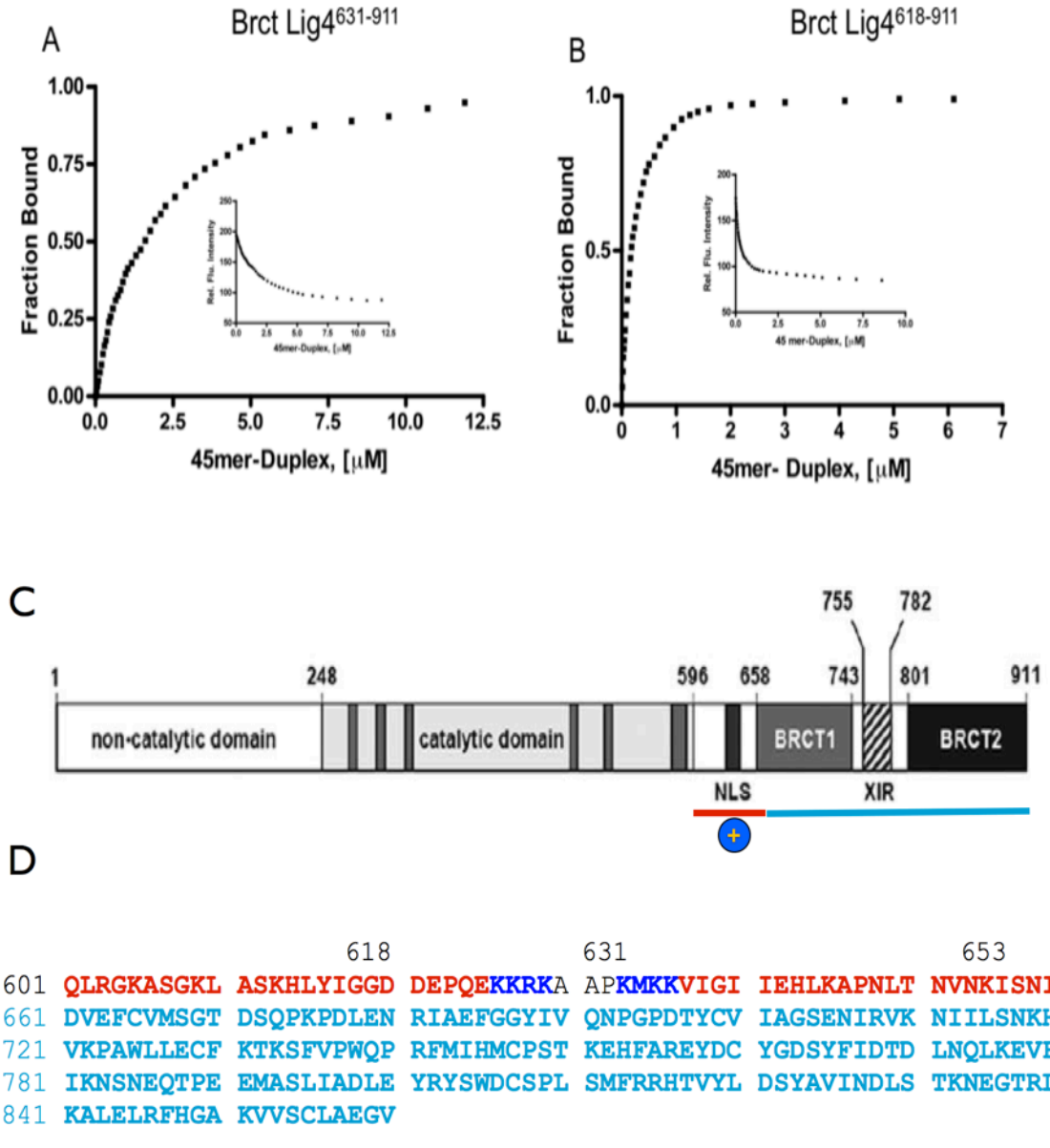

Figure S7. Interaction of BRCT-LigIV with 45bp ds DNA. (A) Fluorescence titration of BRCT-LigIV$^{631-911}$, and (B) BRCT-LigIV$^{618-911}$ complex with duplex 45bp dsDNA. BRCT-LigIV$^{631-911}$ (0.5 μM) and (B) BRCT-LigIV$^{618-911}$ (0.4 μM) in 50 mM Tris-HCl, pH 7.5, 100 mM NaCl, 5 mM $MgCl_2$ and 1 mM DTT, were excited at 295 nm, and the fluorescence intensity was monitored at 335 nm (see insets). The fraction bound, i.e. relative fluorescence (Rel. Fluor.) intensity versus ligand concentration, is plotted. (C) Schematic description of human LigIV (taken from Wu et al, supplementary reference (3)). The region used in our studies is underlined. (D)

Amino acid sequence of C terminus of Lig IV showing basic patches at residues 626-629 and 633-636 in blue. The putative LigIV linker (red) and the BRCT domain (cyan) as defined by Wu, et al, supplementary reference (3) are indicated.

Figure S8

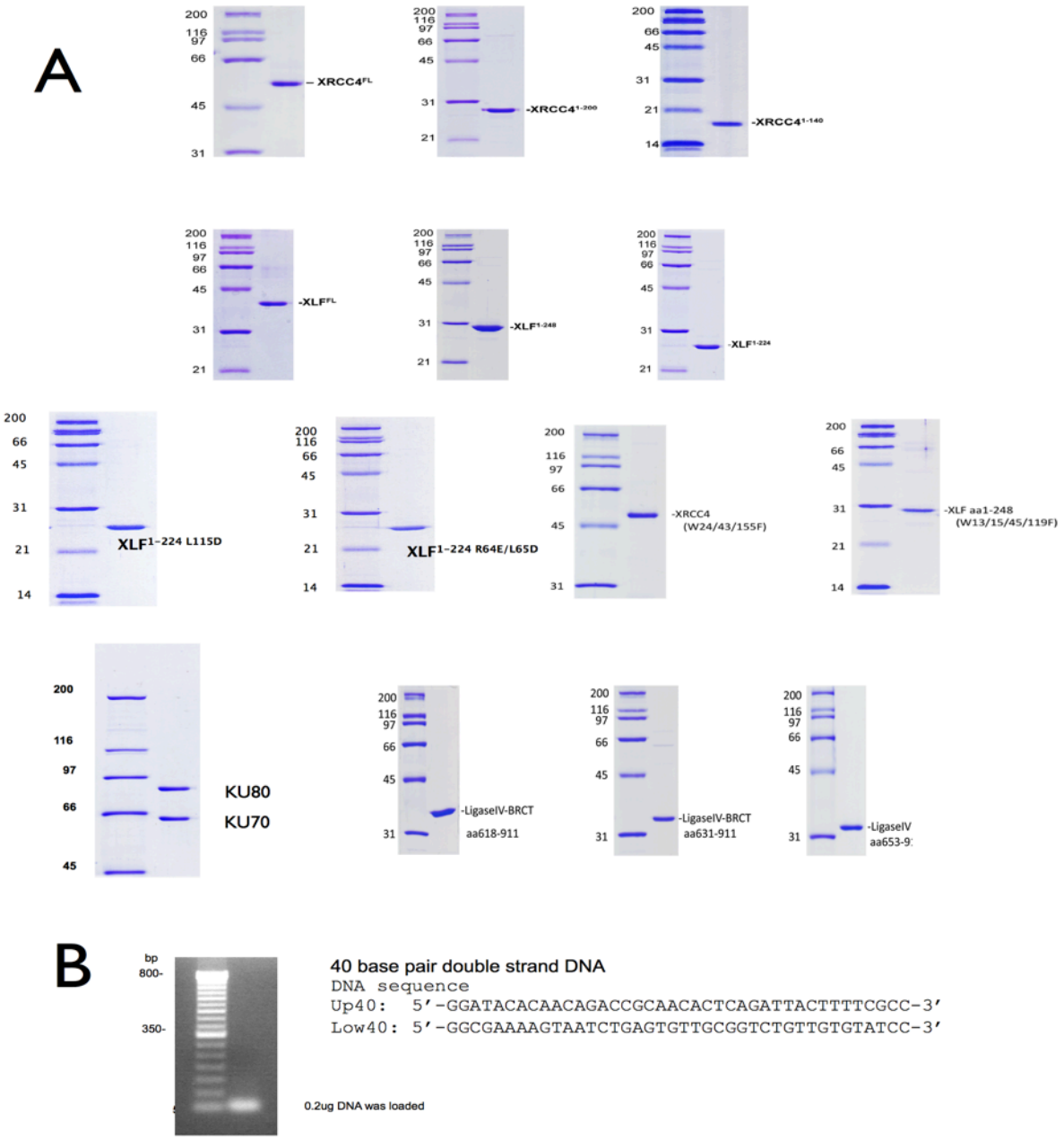

Figure S8. Proteins and DNA used in this study. (A) One µg of each protein was run on SDS PAGE and gels were stained with Coomassie Blue. Molecular weight markers in kDa are shown on the left lane of each gel. (B) Sequence of the 40bpDNA used in this study is shown together with its agarose gel analysis.

Supplementary Experimental Procedures

Protein Purification

Human XLF and XRCC4 were expressed in E. coli as GST-fusion proteins using pGEX-6P-1 vectors (GE Healthcare). Proteins were purified over glutathione sepharose and GST tags were removed as previously described (4,5). Proteins were stored at -80°C in 50 mM Tris-HCl, pH 7.0, 150 mM NaCl, 1 mM EDTA, 1 mM DTT, 1 mM PMSF, 0.2 µg/ml pepstatin and 0.2 µg/ml leupeptin. Constructs used in this study were full length (FL) $XRCC4^{FL}$, $XRCC4^{1-140}$, $XRCC4^{1-200}$, XLF^{FL}, XLF^{1-248}, XLF^{1-224} and XLF^{1-224} containing mutations at L115, R64 and L65, $XRCC4^{FL}$ in which tryptophans at 24, 43 and 155 had been converted to phenylalanine (XRCC4 (W24/43/155F) and XLF^{1-248} in which tryptophans 13, 15, 45 and 119 had been mutated to phenylalanine (XLF^{1-248}(W13/15/45/119F) (Figure S8). After glutathione sepharose chromatography and removal of the GST tag purified XLF^{FL} migrated on SDS PAGE as a doublet of approximately 33 and 40 kDa polypeptides. To further purify XLF^{FL}, protein-containing fractions were diluted to 50 mM salt with buffer containing 50 mM Tris-HCl, pH 8.0, 5% glycerol, 0.2 mM EDTA plus 1 mM DTT, 1 mM PMSF, 0.2 µg/ml leupeptin and 0.2 µg/ml pepstatin, loaded on to a 5 ml Heparin column (GE Healthcare) and eluted using a salt gradient of 50 to 750 mM KCl over 55 minutes at 1 ml/min. Fractions containing a single band of 40 kDa corresponding to XLF^{FL} were pooled and concentrated using a Vivaspin 30 kDa concentrator (GE Healthcare) (Figure S8). Human DNA ligase IV BRCT domain cDNA, corresponding to residues 618-911, 631-911 and 653-911 were amplified from a human HeLa cell cDNA library and subcloned into pGEX6P1 (GE Healthcare), expressed and purified as described above. Primer sequences are available upon request. Ku heterodimer was purified from the nuclear salt wash of unirradiated HeLa cells as described previously (6).

40 bp duplex DNA

A 40-mer deoxy oligonucleotide was synthesized and annealed to form 40bp duplex DNA oligonucleotide. The sequence of the upper strand is shown:
5'-GGATACACAACAGACCGCAACACTCAGATTACTTTTCGCC-3'

Mass shift measurements

Stock solutions of $XRCC4^{1-200}$ and XLF^{1-248} were diluted in buffer (10 mM Tris-HCl, pH 7.5) to equimolar concentrations (50 µM) and incubated at 4ºC for a minimum of 30 min to promote complexation. The sample was held on ice until shift analysis. Aliquots were deuterated for 2 min at 25ºC with the addition of D_2O (25% v/v). Deuteration was quenched by adding the sample to chilled 0.1M glycine-hydrochloride (pH 2.5), and immediately digested by injection into a pepsin microreactor. This microreactor was coupled to an LC-MS system similar to that previously described (7). Briefly, protein digest was captured on a short C18 capillary column and eluted into a Qstar Pulsar i mass spectrometer operated in TOF-MS mode. All fluidic elements, including the microreactor, were held in an ice-bath to minimize deuterium back-

exchange during the analysis time (<15 min). Replicate shift measurements were made (4 or more) and referenced to controls (free XRCC4 and free XLF). All experiments were repeated with the inclusion of 40 bp double-stranded DNA (final concentration 150 μM) as described above. Peptides detected in these analyses were identified by recursive information-dependent acquisitions of MS/MS spectra, until no new identifications were obtained. Spectra were searched against the sequences for $XRCC4^{1-200}$ and XLF^{1-248} using Mascot 2.1. In this fashion, 83 non-redundant peptides for XRCC4 (100% sequence coverage) and 60 non-redundant peptides for XLF (89% sequence coverage) were identified. Sequencing results were manually verified. The average deuterium level for each peptide was determined using Hydra v1.5 (8). Significant shift perturbations were color-coded on the relevant protein structures. Significance in shift perturbations were determined using 1) a two-tailed t test ($p<0.05$) with pooled standard deviations from replicate analyses of free and complexed states 2) a distribution analysis to guard against spectral overlap (9) based on a measurement of the shift noise and assuming its normal distribution. Such data are conveniently portrayed in two-dimensional ΔD vs. 1-p scatterplots (Figure S3A-E) These help avoid determinations of significance on the basis of ΔD alone, and serve to assess the overall quality of the MSP analysis.

Fluorescence Studies

Proteins were dialyzed into 50 mM Tris-HCl (pH 7.5), 100 mM NaCl, 5 mM $MgCl_2$, and 1 mM DTT before each experiment. Fluorescence measurements were carried out on a Perkin-Elmer Life Sciences LS-55 spectrofluorometer equipped with a polarization device using 5-nm spectral resolution for excitation and emission as described in our earlier studies (10). For fluorescence polarization measurements the temperature in the cuvette holder was regulated to 25 °C ± 0.1 °C with an F25 circulating temperature bath from Julabo. The exciting wavelength was 295 nm and the emission was monitored at 335 nm. Following sample equilibration at least 12 data points with an integration time of 5 sec were collected for each data set points.

DNA Docking

Docking calculations were performed with the program DOT (11). The DNA molecule, represented by its atomic positions with partial atomic charges, was systematically moved within the shape and electrostatic potentials calculated for the stationary filament molecule in a rectangular grid 224 x 256 x 288 Å. We used the program MSMS (12) to calculate molecular surfaces, AMBER to assign partial atomic charges, and the program APBS (13) to calculate the electrostatic potentials. From the given 892×10^9 placements, the 200,000 placements with the most favorable interaction energies, calculated as the sum of electrostatics and van der Waals terms, were kept.

Time-dependent SAXS studies

SAXS data were collected at the ALS beamline 12.3.1 (SIBYLS) LBNL Berkeley, California (14). All experiments were performed at 20°C. 16µl of XLF^{1-224}, $XLF^{1-224(L115D)}$, $XLF^{1-224(R64E, L65D)}$ or XLF^{FL} at a concentration of 0.5 mg/ml were exposed for 1s before $XRCC4^{1-140}$ was titrated into the same sample by a pipetting robot. The samples at a 1:1 molar ratio were collected after extensive mixing using the pipetting robot. At least 15 data points were collected with an exposure time of 1 sec with the first data points collected 5s after extensive mixing. Pair distribution functions (P(r)) for each exposure at different time points were calculated by the program GNOM (15). The XRCC4-binding properties were monitored by time-dependent changes in the P(r) function peak at r=85 Å (16). The maximal dimension for the P(r) calculation was fixed for all data points. Possible artifacts arising from X-ray damage were verified by continuous 10s exposures. The continuous 10s exposures showed no increase in the monitored 85 Å P(r) maxima.

Circular Dichroism Spectroscopy

Proteins were dialyzed into 50 mM Tris-HCl (pH 7.5), 100 mM NaCl, 5 mM $MgCl_2$, and 1 mM DTT before each experiment. Circular dichroism measurements were performed in an Olis DSM 17CD spectropolarimeter (Bogart, GA). The temperature in the sample chamber was maintained at 5°C. Each sample was scanned seven times and the experiments were carried out as described previously (17). Protein concentrations used for each determination are presented in the corresponding figure legends.

Supplementary Results and Data Analysis

Supplementary fluorescence experiments: For determination of the DNA binding constant of the XRCC4-XLF complex, XRCC4 and $WFXLF^{1-248}$ (in which all the Trp residues in XLF^{1-248} were replaced by Phe) were initially mixed in 1:1 molar ratio and the observed fluorescence intensity of XRCC4 in this binary complex at 335 nm, following excitation at 295 nm, was taken as the starting control value and the fluorescence titration was carried out as described earlier, by following the changes in emission intensity at 335 nm as a function of 40bp DNA concentration. Analysis of the binding data yielded a K_d value of 0.75 ± 0.05 µM, suggesting that XRCC4 is not only capable of binding duplex DNA in the presence of XLF^{1-248}, but in fact it exhibits slightly higher affinity (K_d of 0.70 µM versus 0.95 µM for XRCC4 by itself) for the duplex DNA.

Supplementary CD analysis: CD spectroscopy can be employed to study protein-protein interactions. Since, the observed ellipticity is an additive parameter, one can generate the theoretical CD spectrum for a mixture of proteins by adding together the spectra of individual proteins, and this spectrum can be compared with that observed experimentally to see whether the interaction has induced any conformational change (10). The far-UV-CD spectra obtained for the [XRCC4-XLF^{FL}] and [XRCC4-XLF$^{1-248}$] complexes (1:1 molar ratios) are shown in Supplementary Figure S4. The experimentally observed ellipticity values deviate from the theoretical values particularly in the 209 and 222-nm wavelength regions, demonstrating that the interaction has produced a conformational change in both complexes. For instance, the difference between the observed and the theoretical ellipticity values at 209 nm for [XRCC4-XLF] and [XRCC4-XLF$^{1-248}$] complexes were ~1500 and ~2400 deg cm^2 dmol^{-1}, respectively, whereas the experimental error in these measurements is only ± 300 deg cm^2 dmol^{-1}. The conformational change induced as a result of interaction of XRCC4 with XLF$^{1-248}$ was significantly larger than that observed with XRCC4 complex with full-length XLF, suggesting that there is little or no interaction between the C-terminal portion of XLF (downstream of residue 248) and XRCC4, in agreement with Malivert et al. (18). Comparison of the secondary structure of the complexes with the secondary structure of the individual proteins suggests that the interaction between XRCC4 and XLF or XLF$^{1-248}$ resulted in a slight increase in the random structure at the expense of the β-structure. Addition of 40-mer duplex DNA to the XRCC4.XLF$^{1-248}$ complex did not induce any significant change in the protein conformation, in agreement with our structural data.

Supplementary References

1. Andres, S. N., Modesti, M., Tsai, C. J., Chu, G., and Junop, M. S. (2007) *Mol. Cell* **28**, 1093-1101
2. Junop, M. S., Modesti, M., Guarne, A., Ghirlando, R., Gellert, M., and Yang, W. (2000) *EMBO J.* **19**, 5962-5970
3. Wu, P. Y., Frit, P., Meesala, S., Dauvillier, S., Modesti, M., Andres, S. N., Huang, Y., Sekiguchi, J., Calsou, P., Salles, B., and Junop, M. S. (2009) Mol. Cell Biol. **29**, 3163-3172
4. Yu, Y., Wang, W., Ding, Q., Ye, R., Chen, D., Merkle, D., Schriemer, D., Meek, K., and Lees-Miller, S. P. (2003) *DNA Repair (Amst)* **2**, 1239-1252
5. Yu, Y., Mahaney, B. L., Yano, K., Ye, R., Fang, S., Douglas, P., Chen, D. J., and Lees-Miller, S. P. (2008) *DNA Repair (Amst)* **7**, 1680-1692
6. Goodarzi, A. A., and Lees-Miller, S. P. (2004) *DNA Repair (Amst)* **3**, 753-767
7. Huzil, J. T., Chik, J. K., Slysz, G. W., Freedman, H., Tuszynski, J., Taylor, R. E., Sackett, D. L., and Schriemer, D. C. (2008) *J. Mol. Biol.* **378**, 1016-1030
8. Slysz, G. W., Baker, C. A., Bozsa, B. M., Dang, A., Percy, A. J., Bennett, M., and Schriemer, D. C. (2009) *BMC Bioinformatics* **10**, 162
9. Chik, J. K., Vande Graaf, J. L., and Schriemer, D. C. (2006) *Anal. Chem.* **78**, 207-214
10. Mani, R. S., Yu, Y., Fang, S., Lu, M., Fanta, M., Zolner, A. E., Tahbaz, N., Ramsden, D. A., Litchfield, D. W., Lees-Miller, S. P., and Weinfeld, M. (2010) *J. Biol. Chem.* **285**, 37619-37629
11. Mandell, J. G., Roberts, V. A., Pique, M. E., Kotlovyi, V., Mitchell, J. C., Nelson, E., Tsigelny, I., and Ten Eyck, L. F. (2001) *Protein Eng.* **14**, 105-113
12. Sanner, M. F., Olson, A. J., and Spehner, J. C. (1996) *Biopolymers* **38**, 305-320
13. Baker, N. A., Sept, D., Joseph, S., Holst, M. J., and McCammon, J. A. (2001) *Proc. Natl. Acad. Sci. U.S.A.* **98**, 10037-10041
14. Hura, G. L., Menon, A. L., Hammel, M., Rambo, R. P., Poole, F. L., 2nd, Tsutakawa, S. E., Jenney, F. E., Jr., Classen, S., Frankel, K. A., Hopkins, R. C., Yang, S. J., Scott, J. W., Dillard, B. D., Adams, M. W., and Tainer, J. A. (2009) Nat. Methods **6**, 606-612
15. Svergun, D. (1992) *J. Appl. Cryst.* **25**, 495-503
16. Hammel, M., Yu, Y., Fang, S., Lees-Miller, S. P., and Tainer, J. A. (2010) *Structure* **18**, 1431-1442
17. Mani, R. S., Karimi-Busheri, F., Fanta, M., Caldecott, K. W., Cass, C. E., and Weinfeld, M. (2004) *Biochemistry* **43**, 16505-16514
18. Malivert, L., Ropars, V., Nunez, M., Devret, P., Miron, S., Faure, G., Guerois, R., Mornon, J. P., Revy, P., Charbonnier, J. B., Callebaut, I., and de Villartay, J. P. (2010) *J. Biol. Chem.* **285**, 26475-26483